

Integrated GIS Technique and Electrical Resistivity Sounding (ERS) for Groundwater Prospecting in Yola Catchment Area, Northern Upper Benue Trough, Nigeria

¹Oniku, A. S., ^{*1,3}Sunu, S. A., ²Nur, A., ¹Timtere, P. and ^{1,4}Kenda, L. P.



¹Department of Physics, Modibbo Adama University, Yola, Adamawa State, Nigeria

²Department of Geology, Modibbo Adama University, Yola

³Department of Petroleum Chemistry & Physics American University of Nigeria (AUN) Yola

⁴Department of Physics, Taraba State University, Jalingo

*Corresponding author's email: abraham.sebastian@aun.edu.ng

ABSTRACT

Groundwater has become an increasingly vital resource in Nigeria, especially in the semi-arid and rapidly growing regions such as the Yola Catchment Area, located in the Northern Upper Benue Trough. The area faces challenges related to water scarcity, population pressure, climate variability, and complex subsurface geologic conditions which necessitate more effective and sustainable groundwater exploration and management strategies. This study, integrated GIS technique and electrical resistivity sounding (ERS) for groundwater prospecting in the Yola catchment area was carried out to identify zones with good potential for groundwater Using the GIS weighted sum and ERS approach. Seven thematic layers; Precipitation, lithology, lineament density, land use/land cover, Drainage network density, soil type, slope, and distance from rivers-were analyzed and weighted by their contribution to groundwater occurrence. Five zones, each representing a different level of groundwater potential, were identified in the area, these are; very poor, poor, low, moderate, and good. Results showed that approximately 21.88% of the area (110.5 km²) has moderate groundwater potential, while the majority (56.56%, or 285.6 km²) falls into the poor category. Areas with very poor and low potential covered 1.19% (6.0 km²) and 18.36% (92.8 km²) respectively, and only 1.99% (10.1 km²) was found to have good potential. Electrical resistivity sounding at five vertical electrical sounding (VES) locations revealed subsurface layers with resistivity values ranging from 10 Ωm to 57 Ωm. Areas with low resistivity ($\leq 20 \Omega\text{m}$) likely indicate clay or water-saturated sediments that restrict water movement, while moderate resistivity values (20–55 Ωm) suggest the presence of silty sands or weathered rock, which may serve as moderate-yield aquifers if porous and saturated.

Keywords:

Aquifers,
Groundwater potential zones,
Electrical resistivity,
Yola Catchment.

INTRODUCTION

Groundwater is a critical natural resource essential for human health, socio-economic development, industrialization, domestic use, and ecological sustainability (UNESCO, 2022; Alley et al., 2002; Famiglietti, 2014). It provides a stable water supply across all climatic regions (Todd & Mays, 2005; Mogaji et al., 2015; Pandey et al., 2020) and is vital in addressing global challenges such as climate change and water scarcity (UN-Water, 2020; IPCC, 2022; UNESCO, 2019). With nearly 99% of liquid freshwater stored in aquifers, groundwater supports over 2.5 billion people worldwide (UNESCO, 2022; Ahmad & Al-Ghouti, 2020; Mishra, 2023). However, increasing demand from

population growth, industrialization, and irrigation, combined with over-extraction and climate impacts, threatens its sustainability (Abijith et al., 2020; Bond et al., 2019; Belhadj et al., 2025).

The Yola catchment area experiences significant water scarcity, exacerbated by seasonal variability and climate change, which lower water tables and hinder irrigation and livelihoods, particularly in the dry season (Sebastian & Adetola, 2022). Growing water demand in this densely populated region necessitates sustainable groundwater exploration and exploitation.

Groundwater occurrence is influenced by a range of physical, climatic, and geological factors, including lithology, slope, soil properties, drainage patterns,

rainfall, and land use (Jha et al., 2010; Chowdhury et al., 2010). Identifying groundwater potential zones (GWPZ) requires an integrated approach. Geographical Information Systems (GIS) and electrical resistivity methods have proven effective for mapping subsurface water-bearing formations (Shahid & Nath, 2002; Singh & Prakash, 2002; Mogaji, 2016; Khan et al., 2021). GIS facilitates spatial data analysis, while resistivity surveys measure subsurface electrical resistance to delineate aquifers. Combined, these technologies enhance the precision of groundwater exploration (Omolaiye et al., 2020; Vasantrao et al., 2017; Taha et al., 2021; Akintorinwa & Okoro, 2019).

Multi-criteria decision analysis within GIS further improves groundwater assessment and site selection (Arulbalaji et al., 2019; Jhariya et al., 2021; Owolabi et al., 2020). Studies confirm that integrating GIS and geophysical methods improves the prediction, management, and sustainable use of groundwater resources (Agbasi et al., 2019; Selvam et al., 2015; Attwa & Zamzam, 2020; Hussein et al., 2017; Abuzed & Alrefaee, 2017).

MATERIALS AND METHODS

Location and Geology of the Study Area

The study area is situated in the northern part of the Upper Benue Trough, specifically within the east–west-trending Yola Basin (also known as the Yola Arm), covering an area of approximately 511.97 km² (Figure 1). Geographically, it lies between latitudes 9°05'N and 9°20'N and longitudes 12°25'E and 12°40'E. The Benue Trough, a major geological feature in Nigeria, is a failed arm of a Cretaceous triple junction rift system (Burke & Dewey, 1973) and is generally divided into Lower, Middle, and Upper sections (Figure 2). The Trough contains up to 6000 meters of sedimentary sequences, ranging from the Cretaceous to the Tertiary periods, with evidence of folding, faulting, and uplift particularly in the pre-mid-Santonian deposits. The Upper Benue Trough comprises three major sub-basins: the Yola Basin (east-west), the Gongola Basin (north-south), and the Lau Basin (northeast-southwest), also known as the Main Arm (Guiraud, 1990; Dike, 2002). The geology and tectonics of the Benue Trough, especially the Upper Benue segment, have been extensively studied (Petters, 1982; Benkhelil, 1982; Dike, 1993, 2002; Obaje, 1994; Zaborski et al., 1997; Zaborski, 2000, 2003).

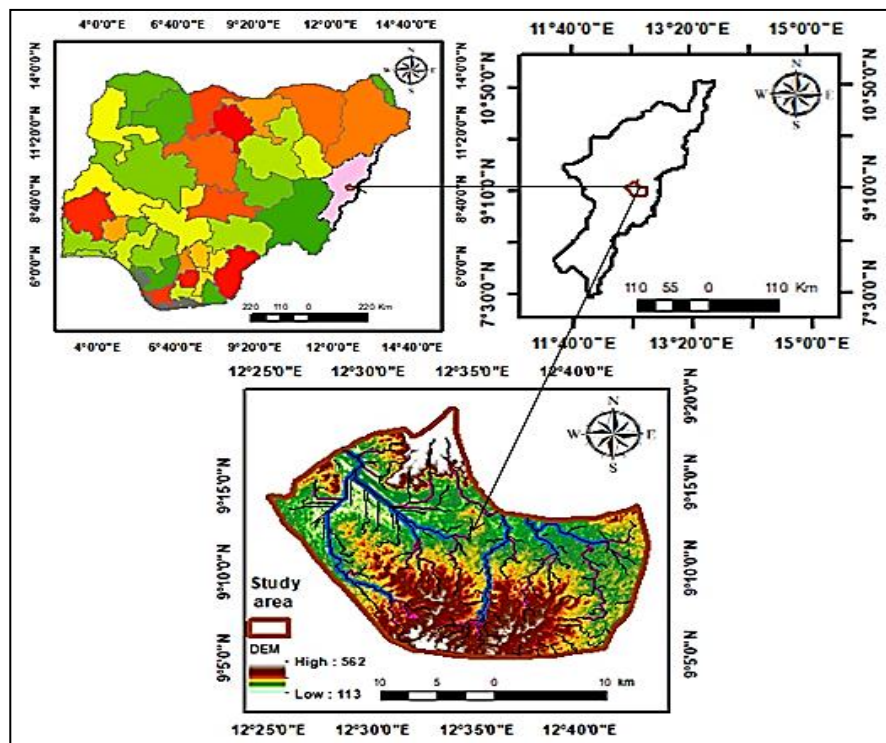


Figure 1: Location map of Yola catchment area (Sebastian et al., 2024)

The stratigraphic sequence of the Upper Benue Trough is depicted in (Figure 3). The oldest deposits belong to the Late Jurassic to Albian Bima Formation, composed of continental sediments that rest unconformably on Precambrian basement rocks. The Bima Formation is

overlain conformably by the Cenomanian-aged Yolde Formation, which transitions from continental to marine environments. This formation consists of basal sandstones and shales, followed by alternating layers of sandstones, shales, and calcareous sandstones.

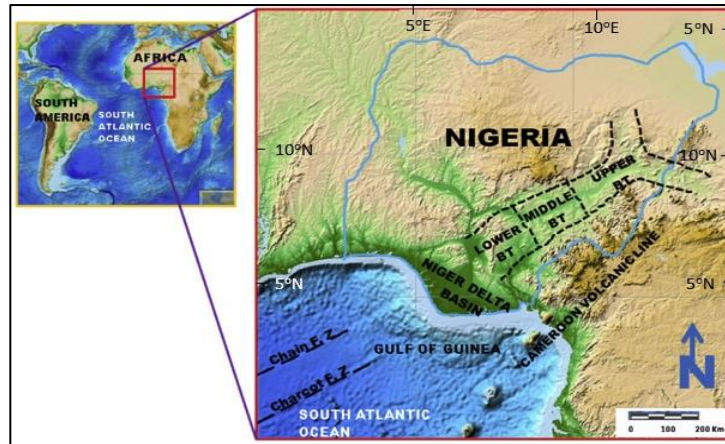


Figure 2: Relief map of Nigeria and Adjoining Areas Showing the Benue Trough (BT) and its Subdivisions. Extracted and Modified from the ETOPO1 Global Relief Model (Amante & Eakins, 2009)

In the Gongola Basin, the sedimentary sequence is dominated by marine successions belonging to the Pindiga and Gongila/Fika Formations. These formations have stratigraphic equivalents in the Yola Basin, namely the Dukul, Jessu, Sekuliye, Numanha, and Lamja Formations. According to Zaborski et al. (1997), the Pindiga Formation is subdivided into five distinct members, reflecting a complex marine depositional history during the Cretaceous period. The youngest Cretaceous sediments in the Upper Benue Trough are

restricted to the Gongola Basin and are represented by the Gombe Formation, a lacustrine to deltaic unit that unconformably overlies older pre-mid-Santonian formations in some areas. The final phase of sedimentation in the Upper Benue Trough is marked by the deposition of the Paleogene Kerri–Kerri Formation, which comprises continental sandstones, siltstones, and shales, indicating a shift to fully continental depositional environments.

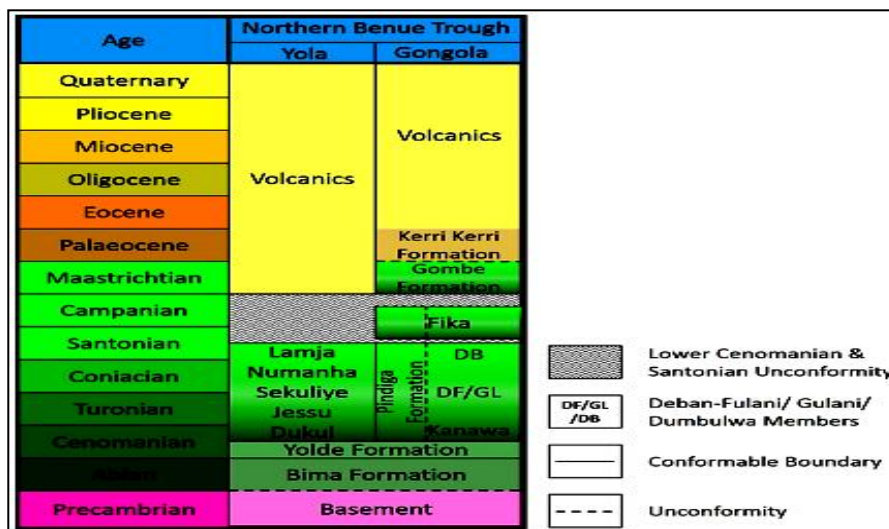


Figure 3: Stratigraphic successions in the Northern Benue Trough after Zaborski (2000) and Dike (1993)

Methodology and Data Acquisition

Data Acquisition Geographic Information System (GIS)

Several geospatial techniques have been used to identify potential groundwater zones within the region of interest (ROI). This includes incorporated digital image

processing, digital elevation model (DEM) assessment, and field studies. To delineate the groundwater potential zone (GPZ) for the study area, eleven key parameters; soil, elevation, geology, rainfall, slope, drainage density, lineament density, distance to the river, land use, and land cover (LULC), watershed, and sub-basin—were

analyzed. The essential dataset for the study, the digital elevation model (DEM), was obtained from the United States Geological Survey (USGS) through the Shuttle Radar Topography Mission (SRTM), with a resolution of 30 meters (cell size = 30 × 30 m/pixel). The DEM was utilized to define the boundaries of the ROI, assess drainage density, and determine the slope using various spatial analysis techniques and tools in ArcGIS 10.6.

Electrical Resistivity Data Acquisition

The resistivity field survey was conducted at multiple locations within the study area using the Schlumberger array. Five Vertical Electrical Sounding (VES) points; VES 001, VES 002, VES 003, VES 004, and VES 005- were carried out with SAS 4000 Tetrameter, employing a maximum current electrode spacing (AB) of 300 meters. This electrode configuration provided valuable insights into the resistivity variation across both shallow and deeper aquifer systems, offering a comprehensive

understanding of subsurface conditions (Telford et al., 1990).

The apparent resistivity for this electrode configuration is calculated using a well-established mathematical expression that accounts for electrode spacing and measured potential difference (Kearey et al., 2002).

$$\rho_a = \frac{V_{MN}}{I} \cdot \pi \left(\frac{\left(\frac{AB}{2}\right)^2 - \left(\frac{MN}{2}\right)^2}{MN} \right) \tag{1}$$

Where ρ_a is the Apparent resistivity (Ωm), AB is the Distance between the two current electrodes (A and B), MN is the Distance between the two potential electrodes (M and N), V is the Measured potential difference (volts), I is the Injected current (amperes), π is the Mathematical constant (≈ 3.1416).

This equation helps in calculating the resistivity of the subsurface, which is then used for interpretation in groundwater and geophysical studies. The resistivity value of different rock formations is given in Table 1.

Table 1: Resistivity values of different rocks

Material	Resistivity (Ωm)
Air	
Pyrite	0.01 - 100
Quartz	500 – 800.000
Calcite	1×10^{12} - 1×10^{13}
Rock Salt	$30 - 1 \times 10^{13}$
Granite	200 – 100.000
Andesite	$1.7 \times 10^2 - 45 \times 10^4$
Basalt	200- 100.000
Limestones	500 – 10.000
Sandstones	200 – 8.000
Shales	20 – 2.000
Sand	1 – 1.000
Clay	1 – 100
Ground Water	0.5 – 300
Sea Water	0.2
Magnetite	0,01 – 1.000
Dry Gravel	600 – 10.000
Alluvium	10 – 800
Gravel	100 – 600

Thematic Map Preparation

Digital Elevation Model (DEM)

A Digital Elevation Model (DEM) is a grid-based, 3D representation of the Earth's surface that records elevation relative to a reference level, such as mean sea level (Burrough & McDonnell, 1998). DEMs are essential in a wide range of applications, including topographic analysis, hydrology, geomorphology, and engineering (Wilson & Gallant, 2000; Moore et al., 1991). In the current study area, elevations range from 149 to 565 meters (Figure 4a), indicating notable topographic variation. This map supports tasks such as slope and aspect analysis, watershed and drainage modeling, and risk assessment (Tarboton, 1997; Hengl &

Reuter, 2009), and their accuracy significantly influences the reliability of spatial analyses (Li et al., 2005).

Slope

The slope is a critical factor influencing groundwater occurrence, affecting water movement, infiltration, and recharge. The Yola landscape features varying terrain, from plains to steep hills. The slope thematic layer for the study area (Figure 4b) was developed using the SRTM DEM (30 × 30 m resolution) in ArcGIS 10.6, with slope percentages ranging from 0% to 90%. The area was classified into five slope categories, with slope class 1 (5-15%) covering 45.12% of the region. A formula (equation 2) for calculating slope percentage was applied

to assess groundwater potential, with steeper slopes limiting recharge and gentler slopes promoting infiltration. Proper slope analysis is essential for sustainable groundwater management and water resource planning.

$$S = \frac{\Delta h}{\Delta d} \times 100 \quad (2)$$

Where S is the Slope percentage (%) Δh is the Change in elevation (vertical rise) (m) and Δd is the Horizontal distance (run) (m)

Rainfall

Rainfall is a key contributor to groundwater recharge, influencing both the quantity and quality of groundwater resources. The amount, intensity, and duration of rainfall determine the volume of water that infiltrates the soil, replenishing aquifers. The rainfall distribution for the study area (Figure 4c) was derived from the CRU TS version 4.07 dataset for the years 2011 to 2020. Rainfall in the region ranges from 9540 mm to 9590 mm annually. In the northern part of the study area, low rainfall occurs from April to June, ranging between 950 mm to 9550 mm, while the southern part experiences higher rainfall from July to September, ranging from 9580 mm to 9590 mm.

Land use/land cover (LU/LC)

Land use and land cover (LULC) significantly influence groundwater occurrence by affecting processes such as infiltration, recharge, and potential contamination. While land use refers to the human utilization of land (e.g., agriculture, urban development), land cover denotes the physical characteristics of the Earth's surface, such as vegetation, water bodies, and bare soil (Lillesand et al., 2015). In this study, satellite imagery was classified using the ESRI Sentinel-2 10-meter Land Use/Land Cover Time Series classification system (Karra et al., 2021). The classification categorized the land into the following classes: Bare ground (0.47%), Built-up area (8.92%), Waterbody (1.83%), Vegetation cover (0.19%), Trees (0.69%), Shrubs (79.05%), Crops (8.82%), and Grass (0.02%) (Figure 4d). These classifications were produced using Impact Observatory's deep learning-based AI land classification model, which was developed in collaboration with ESRI and Microsoft Planetary Computer (Karra et al., 2021).

Distance to River

The proximity to rivers is crucial in influencing groundwater recharge, occurrence, and flow dynamics. Rivers may function as recharge sources or discharge zones for nearby aquifers, depending on the hydraulic gradient between the river and the subsurface water table (Freeze & Cherry, 1979; Todd & Mays, 2005). Understanding this interaction is vital for groundwater resource management, the placement of wells, and flood

risk assessment, especially in regions with variable hydrogeological conditions (Sophocleous, 2002). To assess this influence spatially, a simplified distance-to-river index (D_r) was used (equation 3)

$$D_r = \frac{d}{A} \quad (3)$$

Where D_r is the Distance-to-river index (km/km²) d is the Distance from the river (km), and A = Area of interest (km²). The distance to the river map generated based on equation 3 is as given in Figure 4e.

Watershed

A watershed, also known as a drainage basin or catchment area of land where all surface water converges into a single point (water body), such as a river, lake, or ocean (Figure 4f) was generated for the study area. These watersheds play a crucial role in groundwater occurrence by influencing water infiltration, storage, and recharge. The characteristics of a watershed, including topography, land use, soil type, and vegetation, determine how much water infiltrates into the ground to replenish aquifers (Ward & Robinson, 2000).

Sub-basin

A sub-basin watershed is a smaller division within a larger watershed or drainage basin. Each sub-basin collects and channels water into a main river, lake, or reservoir (Chow et al., 1988). The Sub-basin map of the study area (Figure 4g) was delineated using topographic maps, ArcGIS, and Digital Elevation Models (DEM). The process involves: Identifying Drainage Divides: Using elevation data to map ridgelines, Tracing Tributaries: Identifying smaller streams contributing to larger rivers, Outflow Point Selection; and setting boundaries outlet of the sub-basin. Yola landscape is divided into four subbasins.

Soil

Soil significantly influences groundwater occurrence by regulating water infiltration, percolation, and storage. The soil types map of the study area (Figure 4h) reveals mainly Ferric Luvisols (Lf) covering most parts of the study area characterized by clay soil while the Fluvisols (J) are sand/clay deposits, cover the northern part, and Pellic Vertisols (Vp), mainly alluvium deposits and clay and lithosols (I) are sand, silt /clay not too significant, however, each of the soil type exhibits varying infiltration capacities based on their texture and composition. Sandy soils promote groundwater recharge, while clay-rich soils like Vertisols hinder it due to low permeability and high shrink-swell behavior (Weil et al., 2016; Brady & Weil, 2010; Hillel, 2004).

Structural lineament concentration

Structural lineament concentration is the frequency or density of linear geological features such as faults,

fractures, and joints within a specific area. These structural features often control subsurface fluid movement, making this parameter particularly significant in hydrogeological studies, especially for assessing groundwater potential (Biswas et al., 2012; Rao et al., 2020). These structural features often enhance secondary porosity and permeability, facilitating groundwater flow through otherwise impermeable rock masses (Singhal & Gupta, 2010). Structural lineament concentration is expressed as;

$$L_d = \frac{L}{A} \tag{6}$$

Where L_d is the Structural lineament concentration (km/km²), L is the Total length count Structural lineament concentration in an area (km), and A is the Total location (km²)

The map reveals that the study area is structurally heterogeneous, with prominent zones of high lineament density concentrated in the central and southern parts. These areas may indicate zones of structural weakness, enhanced permeability, or tectonic activity. While the northeastern and northwestern corners show Very Low density (Dark Green), indicating structurally more stable or less fractured zones. Medium-density zones (Yellow) appear to buffer the high and low areas, potentially indicating transitional structural regions.

Geology

Geological formations play a vital role in understanding the distribution and movement of groundwater, as they directly influence the permeability, porosity, and overall structure of the aquifers (Freeze & Cherry, 1979). The lithological properties of rocks and sediments determine the ability of an area to store and transmit water, thus influencing groundwater availability and flow patterns

(Bear, 1979; Domenico & Schwartz, 1990). The geological features of the study area are shown in (Figure 4 j) Precambrian, Metamorphic Rocks (pCm), Cretaceous (KI) Intrusive rocks (e.g., granite, diorite, or gabbro), Cretaceous Sedimentary or Volcanic Rocks (K) shale, sandstone, or limestone and Quaternary Epoch (Qe) Sand, gravel silts, and clays.

Drainage density

Drainage network density is a vital hydrological parameter that quantifies the total length of streams and rivers within a given area (Wang et al., 2015; Schumm, 1956) divided by the area itself. It provides insights into the efficiency of surface runoff and the degree of landscape dissection (Chorley et al., 2019). This parameter plays a significant role in understanding groundwater occurrence because it influences infiltration rates, groundwater recharge, and overall storage potential. In areas with low drainage density, the landscape typically allows for greater water infiltration, promoting groundwater recharge and storage (Figure 4k). In contrast, regions with high drainage density often indicate rapid surface runoff, which may limit groundwater recharge and storage potential.

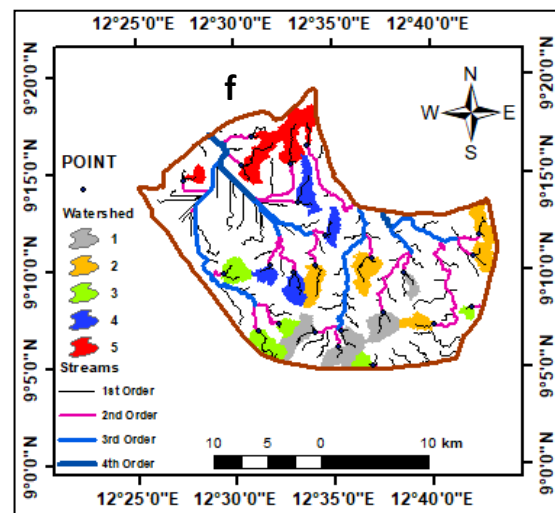
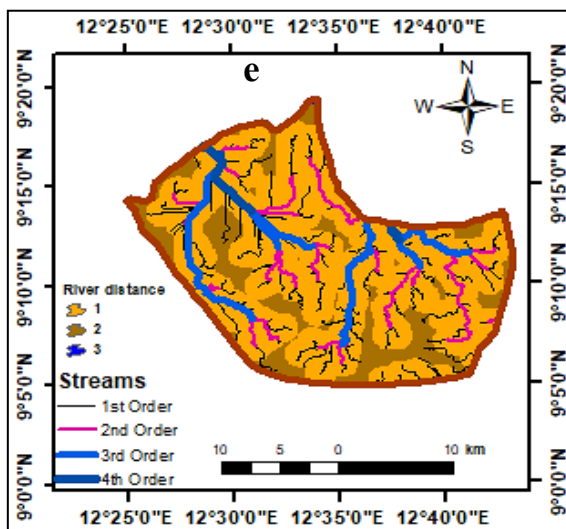
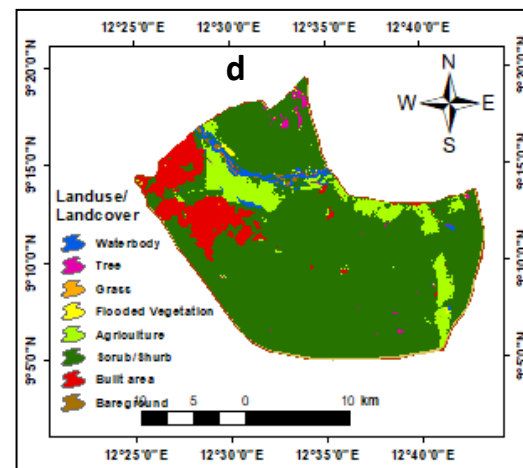
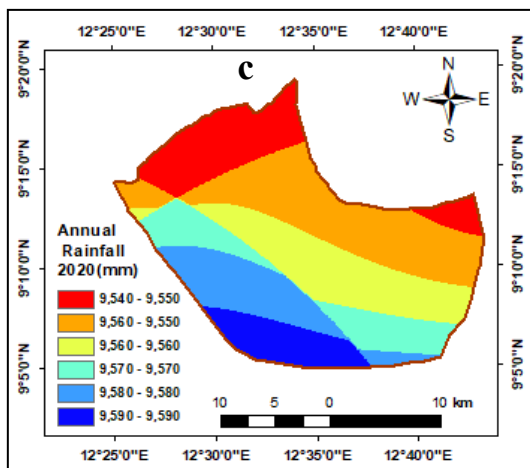
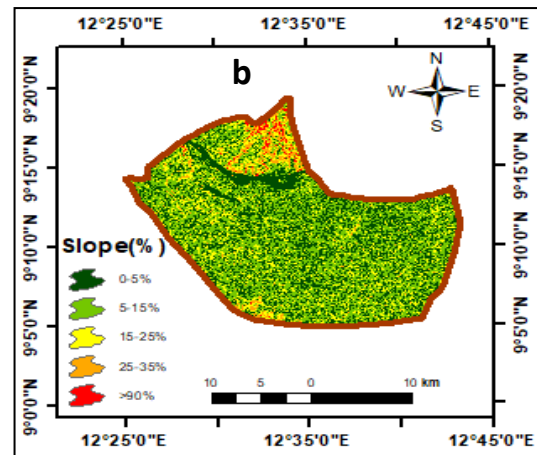
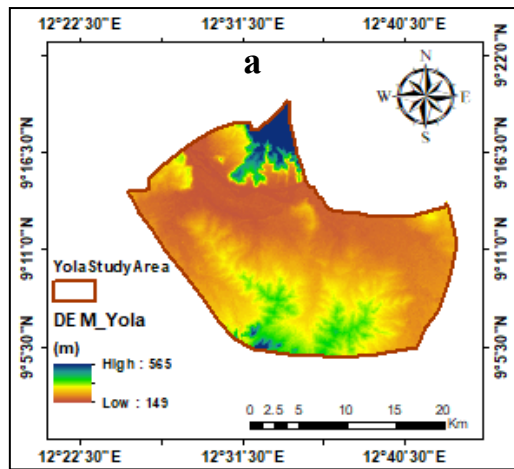
$$\Phi_d = \frac{\ell}{A} \tag{7}$$

Where, Φ_d = Drainage network density (km/km²), ℓ = Total length of all streams and rivers in the basin (km), and A = Total drainage basin area (km²)

Table 2 Represents the weights assigned to different geospatial layers in a groundwater potential index. These weights reflect the relative importance of each factor in influencing the overall outcome or decision-making process. Here's a detailed breakdown of the weight assignment for each thematic layer:

Table 2: Percentage Weightage of Geospatial Layers

S/No	Geospatial layers	% Weight
1	Soil	25.0
2	Slope	20.0
3	Geology	10.0
4	Drainage density	15.0
5	Distance from River	5.0
6	Landuse Land cover (LU/LC)	5.0
7	Rainfall	15.0
8	Lineament Density	5.0



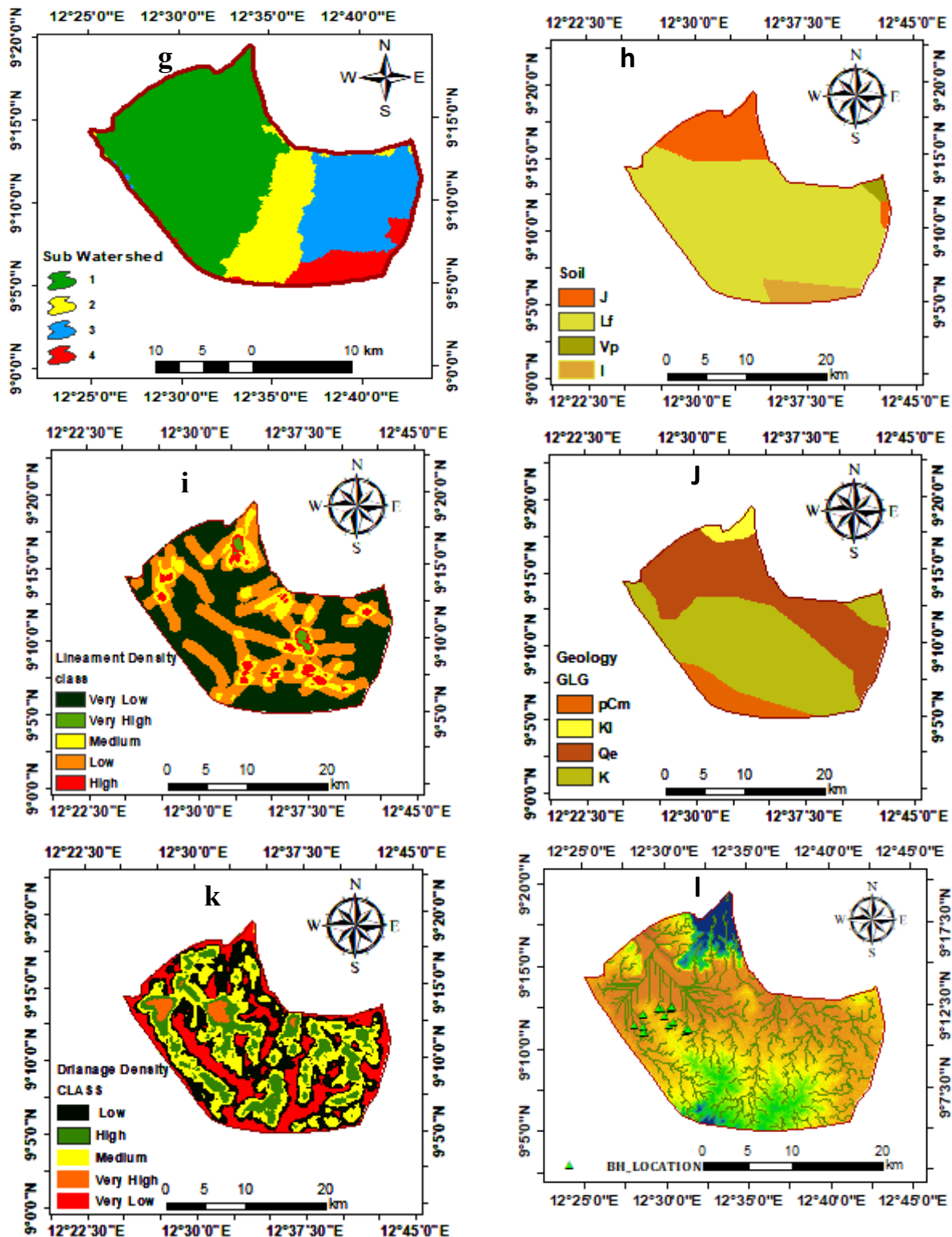


Figure 4: (a) Digital elevation model (b) Slope map (c) Rainfall Map (d) LULC Map (e) Distance to river (f) Watershed Map (g) Sub watershed Map (h) Soil Map (i) Lineament density (j) Geology (k) Drainage density (l) Borehole location

Inversion of resistivity measurements

Forward modeling predicts apparent resistivity for a given resistivity model using the full Schlumberger electrode configuration. A virtual survey, or forward modeling, is performed to generate a predicted dataset based on the initial model. At this stage, the root mean squared (RMS) error at the zeroth iteration is computed.

RESULTS AND DISCUSSION

Groundwater Potential Zones

Groundwater potential zones can be identified by integrating weighted thematic layers and ranked subclasses through the weighted sum overlay method within a GIS framework.

$$GWPZ = \sum_{i=0}^n w_i \times x_i \tag{10}$$

For the number of thematic layers $n = 8$

Where $GWPZ$ is the Groundwater potential zone, w_i is the weight of Element I , $x_i =$ Factor score based on criteria i , and n is the Total count of the thematic layer

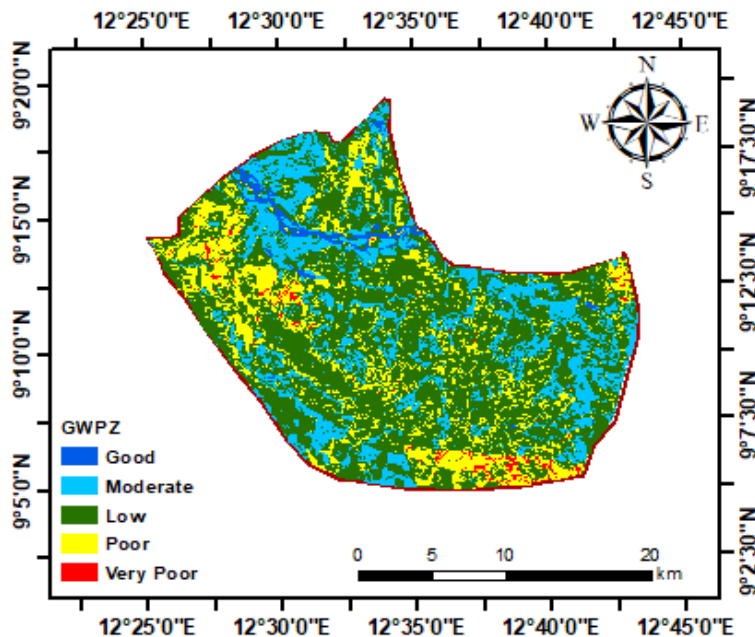


Figure 5: Groundwater-bearing zones in the study area

The resulting Groundwater potential zones of the Yola catchment area have been classified into five groundwater potential zones based on the following: Very poor zone, Poor zone, Low zone, Moderate zone to good potential zone (Table 3). An estimated 110.5 km², representing 21.88% of the study area, has moderate groundwater potential. The majority of the region,

however, was identified as areas having poor groundwater potential, covering 285.6 km² (56.56%). Additionally, areas categorized as very poor, and low groundwater potential account for 6.0 km² (1.19%), and 92.8 km² (18.36%), respectively. Meanwhile, areas with good groundwater potential cover only 10.1 km² (1.99%) of the catchment area.

Table 3: Groundwater potential of Yola catchment area

S/N	Groundwater potential index	Groundwater prospect	Area (km ²)	Percentage covered (%)
1	115 - 222.27	Good	10.1	1.99
2	222.28 - 289.8	Moderate	110.5	21.88
3	289.81 - 321.59	Low	285.6	56.56
4	321.6 - 356.02	Poor	92.8	18.36
5	356.03 - 452.69	Very poor	6.0	1.19

Electrical resistivity curve interpretation for groundwater potential

The measured sounding curves *VES-001*, *VES-002*, *VES-003*, *VES-004*, and *VES-005* correspond to multi-layered models consisting of three layers. The apparent resistivity

data from these soundings were inverted using the EarthImager 1D software, which applies a Newton algorithm for forward modeling to fit 1D field resistivity measurements while minimizing the number of layers needed to perform the inversion. Inverse modeling of

sounding data in EarthImager 1D, a 1D resistivity cross-section was generated, allowing for a comparison of resistivity variations with depth. From this analysis, three distinct layers were identified: Figures 7 a and 8 b VES-001 show measured and modeled layered apparent resistivity respectively, the first layer corresponds to topsoil clay cover with a thickness of 3.7 m with a resistivity value of 28.5 Ωm and weathered zone with a thickness of 5.5 m and 11.5 Ωm resistivity values. The third layer is a partially saturated fractured basement with a recorded resistivity of 34 Ωm with a thickness of 78.8 m; this shows the possibility of groundwater occurrence, in good quantity. Figures 7 c and 8 d VES-002 show measured and modelled layered apparent resistivity respectively, where the first layer corresponds to soil cover with thin compacted clay or fine-grained material of 2.9 m thick with recorded resistivity of 24.6 Ωm, the second layer has low recorded resistivity of 10.5 Ωm with a thickness of 3.0 m which indicate a mixture of clay and sandstone, low recorded resistivity may be attributed to increasing in water retention and mineral content, the third layer is a weathered basement with resistivity value of 49.6 Ωm and thickness of 66 m. Figures 7 e and 8 f VES-003 show measured and modeled layered apparent resistivity indicating a thin consolidated top layer of thickness 3.0 m and recorded resistivity of 30.3 Ωm composed mixture of consolidated clay and sandstone. The second layer is a low resistivity layer of 15.5 Ωm

indicating saturated clay/shale with a thickness of 3.7 m. The third layer is a fractured weathered formation mixed with clay and sandstone with a resistivity of 27.3 Ωm and a thickness of 77.58 m. Figures 7 g and 8 h, present VES-004 a measured and modeled layered apparent resistivity, where the first layer corresponds to compacted soil cover made of clay and sandstone with a resistivity value of 56.6 Ωm and a thickness of 2.9 m, the second layer is compacted weathered clay/sandstone with resistivity value of 30.3Ωm and a thickness of 3.8 m, while the third layer is partially saturated fractured basement rock having recorded resistivity of 34.7 Ωm, with a thickness of 3.7 m; this shows the possibility of groundwater occurrence. Figures 7 i and 8 j, present VES-005 with measured and modeled layered apparent resistivity respectively, where the first layer corresponds to compacted soil cover made of clay with a resistivity of 11.5 Ωm with a thickness of 1.9 m, second layer has recorded resistivity of 26.0 Ωm composed of clay mixed with sandstone with a thickness of 2.0 m, third layer is partially saturated fractured basement with recorded resistivity of 35.9 Ωm with a thickness of 51.1 m. A summary of resistivity and ground water-bearing formations in the Yola catchment area is presented in (Table 4). The VES data interpretation identified only one curve type, namely the H-type, with apparent resistivity $\rho_1 > \rho_2 < \rho_1$

Table 4: Resistivity Interpretation Based on Values from the five VES points obtained from the studies

Resistivity Range (Ωm)	Geological Interpretation
10 - 20 Ωm	Highly conductive layer, likely wet clay, shale, or water-saturated fine sediments
20 - 40 Ωm	Silty sand, weathered rock, or semi-consolidated sediments
40 - 57 Ωm	Sandy formations, lateritic soils, or fractured/weathered rock with freshwater

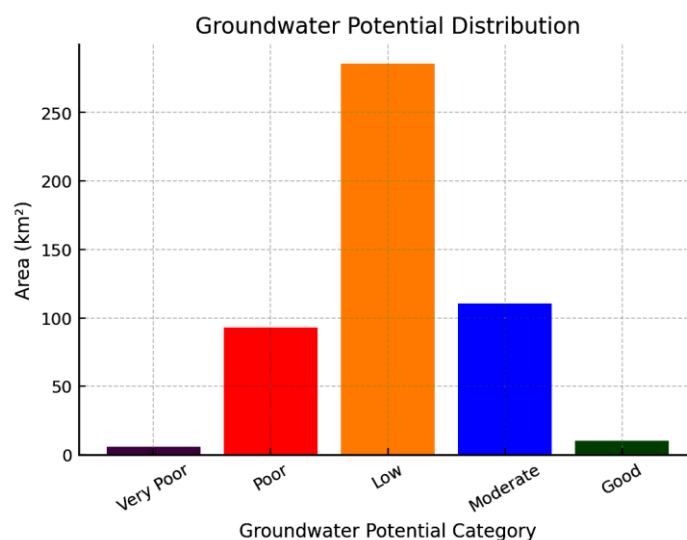
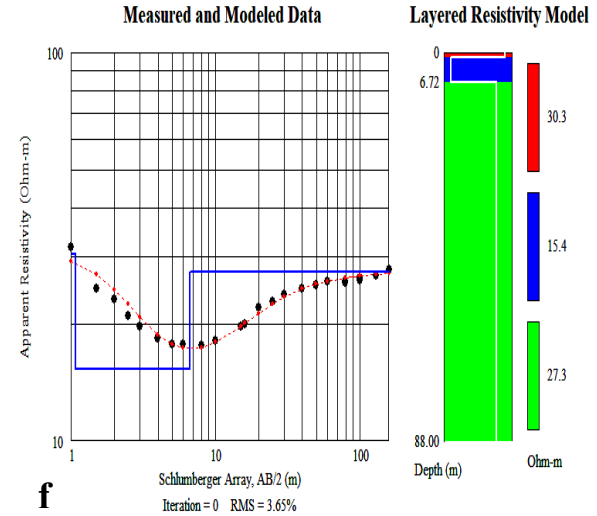
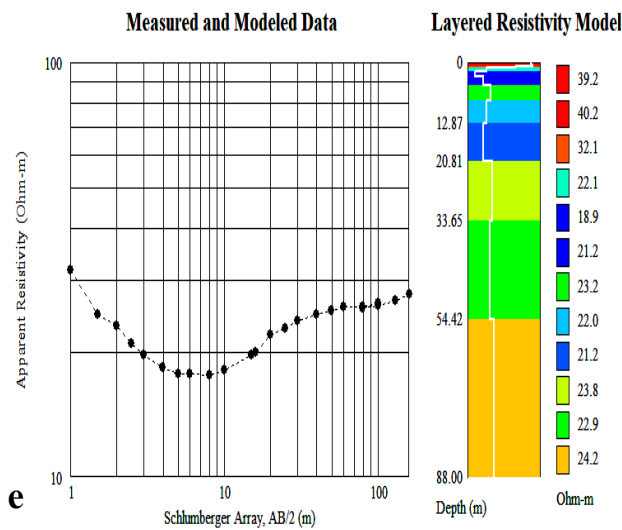
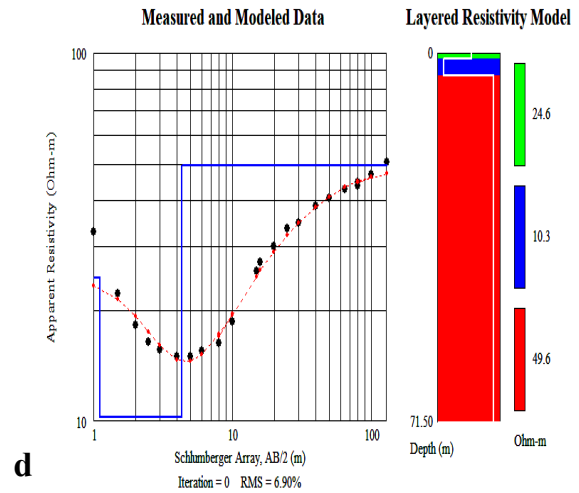
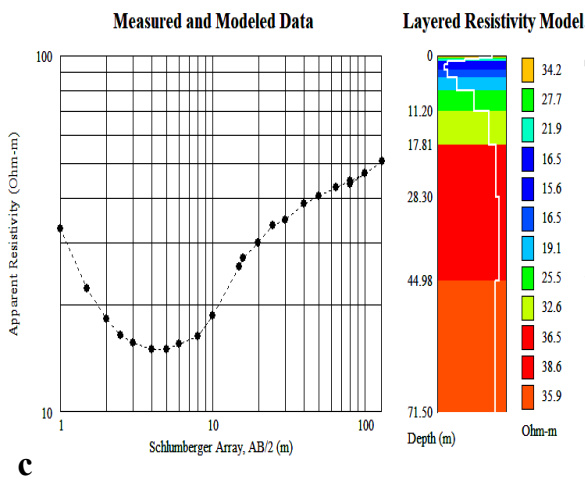
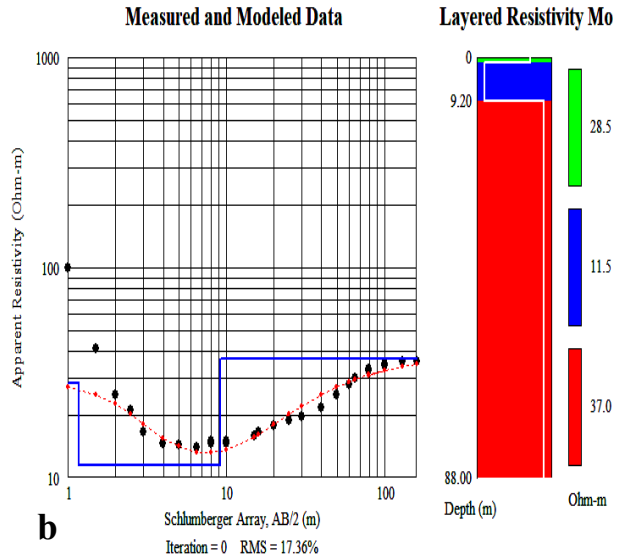
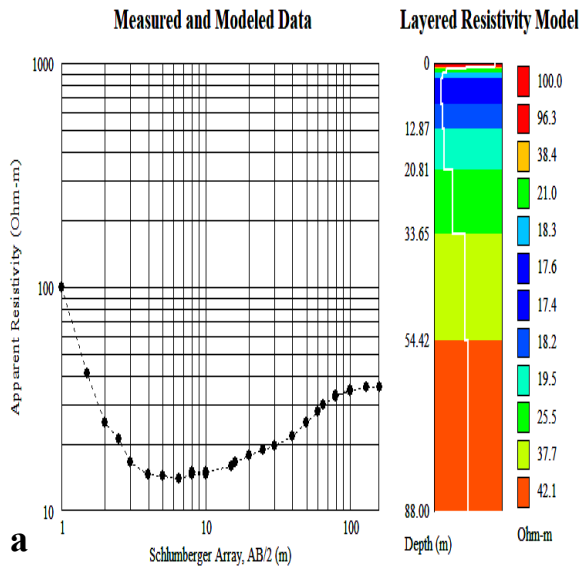


Figure 6: Groundwater potential zone distributions



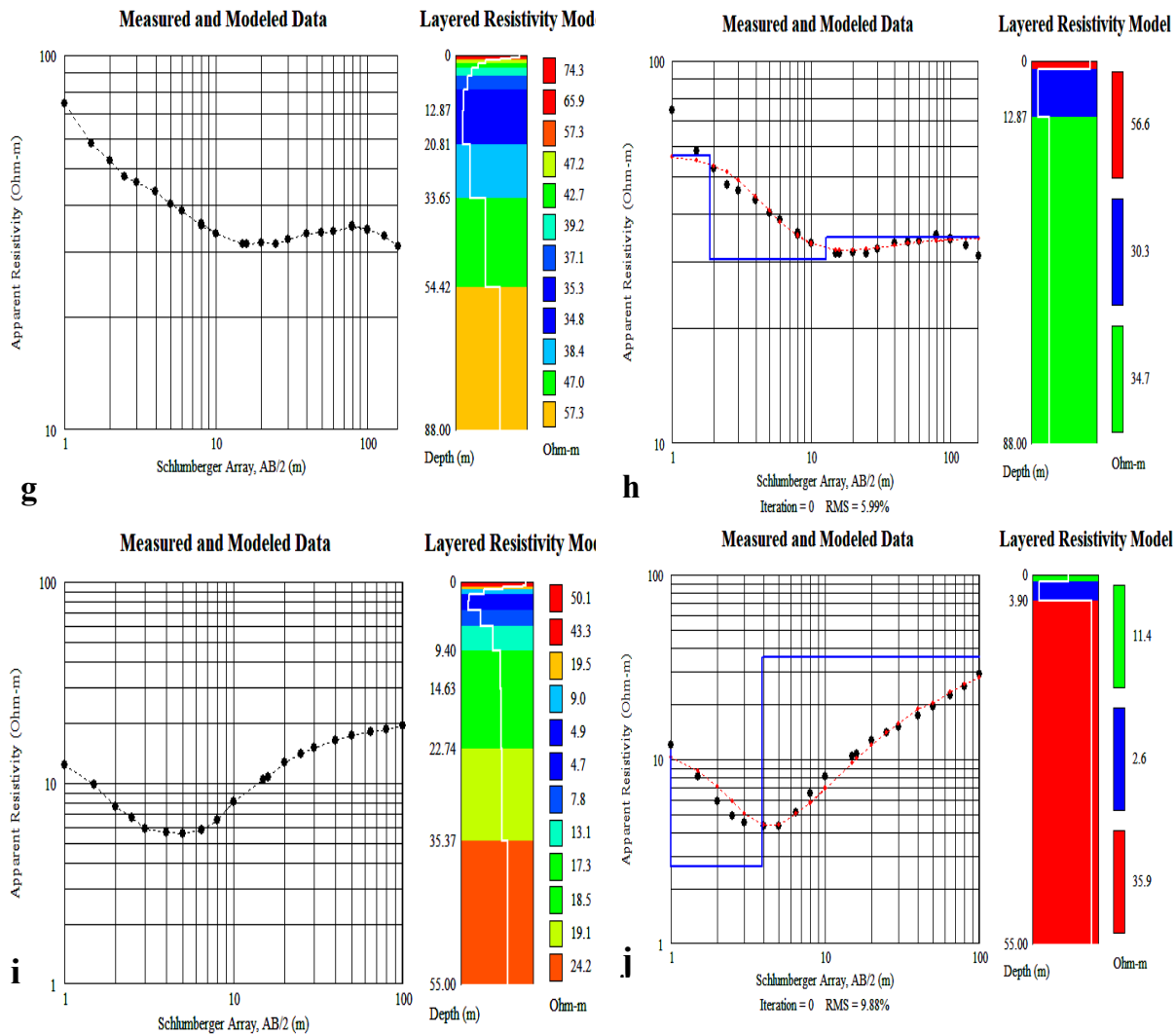


Figure 7: Field curves interpreted results of: (a) VES-001 Observed apparent resistivity (b) VES-001 calculated apparent resistivity and layered model (c) VES-002 measured apparent resistivity (d) VES-002 calculated apparent resistivity and layered model (e) VES-003 measured apparent resistivity (f) VES-003 calculated apparent resistivity and layered model (g) VES-004 measured apparent resistivity (h) VES-004 calculated apparent resistivity and layered model (i) VES-005 measured apparent resistivity (j) VES-005 calculated apparent resistivity and layered model

Table 5: Groundwater-Bearing Formations

Resistivity Range (Ωm)	Possible Lithology	Aquifer Potential
< 20 Ωm	Clay, shale, or saturated fine sediments	Low to negligible – Clay acts as an aquitard, preventing water flow.
20 - 40 Ωm	Silty sand, weathered rock, or semi-consolidated sediments	Moderate – Can hold and transmit groundwater, but yield depends on porosity.
40 - 57 Ωm	Sand, laterite, fractured bedrock	Good – Highly porous formations with potential for freshwater aquifers.

CONCLUSION

This research has shown that GIS techniques can be used to delineate areas with very poor, poor, low, moderate, with good groundwater potential. The major part of the region covering about 285.6 km² (56.56%), was

classified as having poor groundwater while only 1.99% covering about 10.1 km indicates a good groundwater potential zone. The electrical resistivity-sounding results from the studies indicate subsurface strata of three layers with resistivities ranging from 10 Ωm to 57 Ωm across

the five VES points suggesting a mix of clay, sandy, silty, and/or weathered rock formations. The layers detected vary from Clay or alternating layers of loose/consolidated materials that have resistivity $< 55 \Omega\text{m}$, suggesting possible aquifer zones or impermeable clay-rich layers. The highest resistivity $57 \Omega\text{m}$ observed might indicate coarser sands, lateritic material, or fractured bedrock with fresh water. The variation in layer thickness and depth across different VES points indicates lateral heterogeneity in subsurface lithology.

ACKNOWLEDGMENT

The authors wish to thank the Tertiary Educational Trust Fund (TETFund) for providing the grant used for this research through the Institution Based Research (IBR) disbursement. Our gratitude also goes to the reviewers of this work whose inputs have added value to this work.

REFERENCES

Abijith, V. K., Suresh, M., & Elango, L. (2020). Assessment of the impact of urbanization on groundwater resources. *Journal of Earth System Science*, *129*(1), 1–11.

Abuzed, T., & Alrefaee, H. (2017). Integration of GIS and geoelectrical techniques for groundwater assessment in arid regions. *Arabian Journal of Geosciences*, *10*(22), 499.

Agbasi, O. E., Aziz, N. A., Abdulrazzaq, Z. T., & Etuk, S. E. (2019). Integrated geophysical data and GIS technique to forecast the potential groundwater locations in part of South Eastern Nigeria. *Iraqi Journal of Science*, *60*(5), 1013–1022.

Ahmad, M., & Al-Ghouti, M. A. (2020). Groundwater: Occurrence, quality, and management. In *Water and Sustainable Development* (pp. 47–68). Springer.

Akintorinwa, O. J., & Okoro, A. I. (2019). Geophysical investigation for groundwater potential in a basement complex terrain. *Journal of African Earth Sciences*, *151*, 144–154.

Alley, W. M., Reilly, T. E., & Franke, O. L. (2002). *Sustainability of groundwater resources* (U.S. Geological Survey Circular 1186). U.S. Geological Survey.

Arulbalaji, P., Padmalal, D., & Maya, K. (2019). AHP and GIS-based approach for delineating groundwater potential zones in the complex hard rock terrain of Western Ghats, India. *Applied Water Science*, *9*(3), 1–17.

Attwa, M., & Zamzam, M. (2020). Integrated approach using geophysical and hydrochemical data for groundwater exploration. *HydroResearch*, *3*, 28–38.

Bear, J. (1979). *Hydraulics of groundwater*. McGraw-Hill.

Belhadj, M., Chenini, I., & Bouri, S. (2025). Global access to safe drinking water: Trends, challenges, and prospects. *Environmental Challenges*, *10*, 100573.

Benkhelil, J. (1982). Benue Trough and Benue Chain. *Geological Magazine*, *119*(2), 155–168. <https://doi.org/10.1017/S0016756800025842>

Biswas, A., Sharma, S. P., & Kumar, A. (2012). Delineating prospective groundwater zones in hard rock terrain from electrical resistivity and VES data. *Hydrogeology Journal*, *20*(4), 743–755. <https://doi.org/10.1007/s10040-012-0845-2>

Bond, N. R., Costelloe, J. F., King, A. J., & Warfe, D. M. (2019). Managing freshwater flows for the environment in a changing climate. *Marine and Freshwater Research*, *70*(8), 1101–1113.

Brady, N. C., & Weil, R. R. (2010). *Elements of the nature and properties of soils* (3rd ed.). Prentice Hall.

Burke, K., & Dewey, J. F. (1973). Plume-generated triple junctions: Key indicators in applying plate tectonics to old rocks. *The Journal of Geology*, *81*(4), 406–433.

Burrough, P. A., & McDonnell, R. A. (1998). *Principles of geographical information systems* (2nd ed.). Oxford University Press.

Chorley, R. J., Schumm, S. A., & Sugden, D. E. (2019). *Geomorphology*. Routledge.

Chowdhury, A., Jha, M. K., & Chowdhary, V. M. (2010). Delineation of groundwater recharge zones and identification of artificial recharge sites in West Medinipur district, West Bengal, using RS, GIS, and MCDM techniques. *Environmental Earth Sciences*, *59*(6), 1209–1222.

Dhakate, R., Singh, V. S., & Mohanty, B. P. (2016). Integrated geophysical techniques for groundwater prospecting in hard rock terrains. *Journal of Hydrology*, *540*, 774–785.

Dike, E. F. C. (1993). Stratigraphy and structure of the Kerri–Kerri Basin, Upper Benue Trough, Northeastern Nigeria. *Journal of Mining and Geology*, *29*(2), 77–93.

- Dike, E. F. C. (2002). Sedimentation and tectonic evolution of the Upper Benue Trough and Bornu Basin, northeastern Nigeria. *Journal of Mining and Geology*, 38(2), 155–168.
- Domenico, P. A., & Schwartz, F. W. (1990). *Physical and chemical hydrogeology*. John Wiley & Sons.
- Famiglietti, J. S. (2014). The global groundwater crisis. *Nature Climate Change*, 4(11), 945–948.
- Freeze, R. A., & Cherry, J. A. (1979). *Groundwater*. Prentice-Hall.
- Guiraud, R. (1990). Tectono-sedimentary framework of the Early Cretaceous continental Bima Formation, Upper Benue Trough, NE Nigeria. *Journal of African Earth Sciences*, 10(1/2), 341–353. [https://doi.org/10.1016/0899-5362\(90\)90101-0](https://doi.org/10.1016/0899-5362(90)90101-0)
- Gyeltshen, S., Dorji, P., & Tshering, L. (2020). Groundwater potential zonation using GIS and remote sensing techniques. *Hydrology*, 7(1), 13.
- Hengl, T., & Reuter, H. I. (Eds.). (2009). *Geomorphometry: Concepts, software, applications*. Elsevier.
- Hillel, D. (2004). *Introduction to environmental soil physics*. Academic Press.
- Hussein, M., Gharib, A. F., & Abdelrahman, E. M. (2017). Integrating remote sensing and geoelectrical data for groundwater exploration. *Journal of African Earth Sciences*, 134, 714–727.
- IPCC. (2022). *Climate Change 2022: Impacts, Adaptation and Vulnerability*. Intergovernmental Panel on Climate Change.
- Jha, M. K., Chowdary, V. M., & Chowdhury, A. (2010). Groundwater assessment in a hard rock region using geoinformatics. *Environmental Monitoring and Assessment*, 166(1), 537–556.
- Jhariya, D. C., Champati Ray, P. K., & Patel, N. R. (2021). Delineation of groundwater potential zones using AHP and GIS. *Applied Water Science*, 11(3), 1–14.
- Karra, K., Kontgis, C., Statman-Weil, Z., Mazzariello, J. C., Mathis, M., & Brumby, S. P. (2021). Global land use/land cover with Sentinel-2 and deep learning. In *Proceedings of the IEEE International Geoscience and Remote Sensing Symposium (IGARSS)* (pp. 4704–4707). IEEE. <https://doi.org/10.1109/IGARSS47720.2021.9553493>
- Kearey, P., Brooks, M., & Hill, I. (2002). *An introduction to geophysical exploration* (3rd ed.). Wiley-Blackwell.
- Khan, S., Shankar, R., & Kumar, R. (2021). Assessment of aquifer potential using vertical electrical sounding in alluvial terrain. *HydroResearch*, 4, 27–34.
- Li, Z., Zhu, C., & Gold, C. (2005). *Digital terrain modeling: Principles and methodology*. CRC Press.
- Lillesand, T. M., Kiefer, R. W., & Chipman, J. W. (2015). *Remote sensing and image interpretation* (7th ed.). Wiley.
- Mishra, K. (2023). Importance of groundwater in sustainable water management. *Water Resources Management*, 37(1), 45–59.
- Mogaji, K. A. (2016). GIS-based geoelectrical assessment of aquifer potential. *Journal of African Earth Sciences*, 121, 274–288.
- Mogaji, K. A., Lim, H. S., & Abdullahi, U. M. (2015). Statistical evaluation of groundwater potential in a basement complex terrain. *Environmental Earth Sciences*, 74(10), 7067–7080.
- Mohamed, A. A., Mahmoud, S. H., & Alazba, A. A. (2023). Integrated geophysical investigations for sustainable groundwater development. *Groundwater for Sustainable Development*, 20, 100809.
- Moore, I. D., Grayson, R. B., & Ladson, A. R. (1991). Digital terrain modelling: A review of hydrological, geomorphological, and biological applications. *Hydrological Processes*, 5(1), 3–30. <https://doi.org/10.1002/hyp.3360050103>
- Obaje, N. G. (1994). Coal petrography, microfossils and palaeoenvironments of Cretaceous coal measures in the Middle Benue Trough of Nigeria. *Tectonophysics*, 7(3), 245–263.
- Omolaiye, A. M., Oladunjoye, M. A., & Amadi, A. N. (2020). Delineation of groundwater potential zones using GIS and geoelectrical resistivity data. *Environmental Earth Sciences*, 79, 78.
- Owolabi, O. A., Akinlalu, A. A., & Adewumi, T. O. (2020). GIS-based groundwater potential mapping in crystalline basement terrain. *Heliyon*, 6(9), e04887.
- Pandey, P., Himanshu, S. K., & Mishra, S. K. (2020). Groundwater recharge estimation using remote sensing

- and GIS techniques: A case study. *Sustainable Water Resources Management*, 6(3), 1–12.
- Petters, S. W. (1982). Central West African Cretaceous-Tertiary benthic foraminifera and stratigraphy. *Palaeontographica Abteilung A*, 179(1–3), 1–104.
- Rao, S. M., Sarma, V. S., & Radhakrishna, M. (2020). Identification of groundwater potential zones using remote sensing and GIS techniques: A case study of Siddipet district, Telangana, India. *Applied Water Science*, 10(7), 1–14. <https://doi.org/10.1007/s13201-020-01234-7>
- Reynolds, J. M. (2011). *An introduction to applied and environmental geophysics* (2nd ed.). Wiley-Blackwell.
- Schumm, S. A. (1956). Evolution of drainage systems and slopes in badlands at Perth Amboy, New Jersey. *Geological Society of America Bulletin*, 67(5), 597–646. [https://doi.org/10.1130/0016-7606\(1956\)67\[597:EODSAS\]2.0.CO;2](https://doi.org/10.1130/0016-7606(1956)67[597:EODSAS]2.0.CO;2)
- Sunu, F., & Adetola, M. O. (2022). Impacts of climate variability on groundwater resources in Yola Catchment. *Nigerian Journal of Environmental Sciences and Technology*, 6(2), 82–91.
- Selvam, S., Dhivakar, S., & Magesh, N. S. (2015). Groundwater potential zone identification using remote sensing and GIS. *Arabian Journal of Geosciences*, 8, 867–875.
- Shahid, S., & Nath, S. K. (2002). GIS integration of remote sensing and geophysical data for groundwater exploration. *Journal of Spatial Hydrology*, 2(2), 1–14.
- Singh, P. K., & Prakash, A. (2002). Delineation of groundwater potential zones using remote sensing and GIS. *Journal of the Indian Society of Remote Sensing*, 30(4), 197–204.
- Singh, S. K., Panda, S. N., & Kumar, A. (2018). Integrated geospatial techniques for groundwater prospect mapping. *Journal of Environmental Management*, 207, 101–112.
- Singhal, B. B. S., & Gupta, R. P. (2010). *Applied hydrogeology of fractured rocks* (2nd ed.). Springer.
- Sophocleous, M. (2002). Interactions between groundwater and surface water: The state of the science. *Hydrogeology Journal*, 10(1), 52–67. <https://doi.org/10.1007/s10040-001-0170-8>
- Taha, A. M., Ahmed, A. I., & Zaki, A. S. (2021). Integration of geophysical and GIS techniques for groundwater evaluation. *HydroResearch*, 4, 54–66.
- Tarboton, D. G. (1997). A new method for the determination of flow directions and upslope areas in grid digital elevation models. *Water Resources Research*, 33(2), 309–319. <https://doi.org/10.1029/96WR03137>
- Telford, W. M., Geldart, L. P., & Sheriff, R. E. (1990). *Applied geophysics* (2nd ed.). Cambridge University Press.
- Todd, D. K., & Mays, L. W. (2005). *Groundwater hydrology* (3rd ed.). Wiley.
- UNESCO. (2019). *The United Nations World Water Development Report 2019: Leaving No One Behind*. United Nations Educational, Scientific and Cultural Organization.
- UNESCO. (2022). *The United Nations World Water Development Report 2022: Groundwater: Making the Invisible Visible*. United Nations Educational, Scientific and Cultural Organization.
- UN-Water. (2020). *Water and Climate Change*. United Nations. Vasantrao, B. B., Suresh, S., & Krishna, P. M. (2017). Delineation of groundwater potential zones using geoinformatics. *Applied Water Science*, 7(8), 4331–4341.
- Wang, X., Yang, T., & Wang, Y. (2015). Relationship between drainage density and rainfall-runoff processes: A case study in a semi-arid basin. *Water*, 7(12), 6931–6948. <https://doi.org/10.3390/w7126665>
- Ward, R. C., & Robinson, M. (2000). *Principles of hydrology* (4th ed.). McGraw-Hill.
- Weil, R. R., Brady, N. C., & Weil, R. R. (2016). *The nature and properties of soils* (15th ed.). Pearson.
- Wilson, J. P., & Gallant, J. C. (2000). *Terrain analysis: Principles and applications*. Wiley.
- Zaborski, P. (2000). Cretaceous stratigraphy, paleogeography and tectonism of the southern parts of the Upper Benue Trough, Nigeria. *Bulletin des Centres de Recherches Exploration-Production Elf-Aquitaine*, 22(1), 153–165.
- Zaborski, P. (2003). Guide to the Cretaceous paleogeography of the Upper Benue Basin. *NAPE Bulletin*, 15(1), 23–42.

Zaborski, P., Ugodulunwa, F., Idornigie, A., Nnabo, P., & Ibe, K. (1997). The Cretaceous and Paleogene Sedimentary Basins of Nigeria. *Nigerian Mining and Geosciences Society Bulletin*, 32, 1–97.

Zaher, M., El-Kelani, R., & Hamed, Y. (2021). Integrated geophysical methods for groundwater assessment in arid environments. *Journal of African Earth Sciences*, 180, 104205.